Short Communication

Microstructural verification of the theoretically predicted morphologies of the NiAl–Cr pseudo-binary alloy systems and NiAl–Cr eutectic structure modification by Mo addition

C. Mathiou[1] · K. Giorspyros[1] · E. Georgatis[1] · A. E. Karantzalis[1]

Abstract
Based on the NiAl–Cr pseudo-binary phase diagram, ranging from hypo- to hyper-eutectic areas, alloys with various compositions were produced by arc melting. The microstructures were compared with the theoretical predictions of Tang et al. (Chem Chem Phys 18(29):19773–19786, 2016) and they were proved to be in agreement. The partial substitution of Cr by Mo in three different compositions revealed eutectic and hypo-eutectic microstructures with the eutectic micro-constituent modified from fibrous to lamellar. The importance of T0-A2 and T0-B2 temperatures [the maximum temperatures under which, partitionless solidification of A2 and B2 phases respectively happens (Laughlin and Hono in Physical metallurgy, Elsevier, Amsterdam, 2014)] and their relation to Te (eutectic temperature) proved to be the dominant factor that shifts the microstructures to off equilibrium morphologies in the case of NiAl–Cr alloys.

Keywords NiAl–Cr system · Medium entropy alloys · Eutectic modification · Solidification

1 Introduction

During the last decade, significant research effort has been conducted in the field of NiAl based alloy and composite systems. NiAl having a density of 5.9 g/cm^3 (stoichiometric NiAl), a coefficient of thermal expansion comparable to that of Ni-base superalloys [3] and a high degree of thermodynamic stability as evident from its very large negative enthalpy of mixing − 22 kJ/mol [3] (thus easy to fabricate in various forms), made NiAl alloys potential and attractive candidates for high temperature applications in an effort to substitute various categories of existed super-alloys [1, 4, 5]. The NiAl–Cr system, as part of this effort, has attracted special interest [6]. Apart from, nevertheless, this specific field of super-alloy potential substitution, the appearance of high entropy alloys at the metallurgical research fronts, revealed another dimension of the importance of the Ni–Al–Cr elemental combination. A significant amount of these new class alloys has been developed and assessed based on this Ni–Al–Cr core [7–12]. These research efforts made clear the necessity for a thorough understanding of the microstructural features—and the related to them formation mechanisms and phenomena—of the NiAl–Cr systems. Even more, the addition of other elements and the adoption of special techniques aiming to the strength increase, has also been recorded. At previous works, Cline and Walter [13] showed that the Mo addition to the NiAl–Cr eutectic alloy modifies the microstructure from Cr fibers to Cr(Mo) lamellae. Demirtas and Gungor [14] presented in their work on the NiAl–28Cr–6Mo, the mechanical properties after adding small quantities of Fe, Nb, Ti and heat treatment of the produced alloys. Shang et al. [15] studied the microstructure and the room fracture toughness of NiAl–32Cr–6Mo and Yang et al. [16] have produced similar alloys. They used directional solidification techniques to control the solidification rate. Zang et al. [17]

✉ A. E. Karantzalis, akarantz@uoi.gr | [1]Department of Materials Science and Engineering, University of Ioannina, Ioannina, Greece.

SN Applied Sciences (2019) 1:1292 | https://doi.org/10.1007/s42452-019-1338-y

Received: 3 August 2019 / Accepted: 23 September 2019 / Published online: 27 September 2019

produced near eutectic NiAl–Cr–Mo alloys with Ti, Hf, Nb and W additions. This work aimed to create conditions of no fibrous solidification of Cr in the NiAl–Cr–Mo system and, by this approach, to increase the strength of the NiAl–Cr–Mo eutectic or near eutectic alloys. Wang et al. produced NiAl–Cr(Mo) hyper-eutectic alloys using directional solidification techniques aiming to lamellar solidification of Cr(Mo) in the eutectic micro-constituent [18]. Additionally, Zheng et al. [19] and Sheng et al. [20] has extensively investigated the effect of elemental additions, such as Ho and Hf in the first case and Hf and Dy in the second, on the microstructure and the mechanical properties of the basic NiAl–Cr(Mo) core. In the case of Ho and Hf addition [19] the researchers distinguished their synergetic action which caused multiple intermetallic phase precipitation sequences, morphological alterations of the eutectic structures and primary phases and improvement in micro-hardness and strength. In the case of Hf and Dy additions [20] the authors showed apart formation of various precipitates, a possibility of microstructural refinement and tuning leading to a significant improvement of the mechanical response.

Tang et al. [1] presented an exceptional research effort on clarifying the possible microstructural configurations of the NiAl–Cr system at various compositions, based on thermodynamic and kinetic calculations. This is exactly where this current report aims to contribute: The authors attempted an experimental verification of the theoretical predictions proposed by Tang et al. [1] at off equilibrium conditions. They produced the alloys by arc melting technique where the solidification rate is high as it takes place on a water-cooled cooper-base crucible. The novelty of the present effort is exactly associated with the use of solidification considerations to explain the obtained microstructures: at the best of the authors knowledge no such systematic approach based on the recalescence, undercooling, partitioning/partitionless growth temperatures T0 is reported in the literature for the NiAl–Cr based systems.

They also produced three more alloys in eutectic or near eutectic composition by partially substituting Cr with Mo. The microstructure evolution under fast solidification conditions of these alloys is one of the aims of the present work. This effort and the described results, are part of an ambitious wide project currently being undertaken, which aims to expand the initial NiAl–Cr core to a step by step building of medium- and high-entropy alloy systems towards two different directions: (a) a systematic approach of designing refractory-transition metals medium and high entropy alloy systems through the addition of various refractory metals (Mo, W etc.) to the basic NiAl–Cr core and (b) a systematic approach of designing medium and high entropy alloy systems of controllable ductility and strength by the additions of various elements such as Fe, Mn, Co, Ti etc.

2 Experimental procedure

High purity elemental powders were mixed in the intended atomic ratio in order to produce the various Ni–Al–Cr alloys and Ni–Al–Cr–Mo alloys. Approximately 5 g of raw materials, with purities higher than 99.5%, were subjected to uniaxial compression in order to make green pellets with targeted composition according to Tables 1 and 2. The produced green pellets were arc melted at least 5 times in order to ensure that all raw materials were well mixed in liquid prior to solidification. The melting was performed on a specially formed cavity on the surface of a water-cooled copper base. The shape of the samples was that of a meniscus. The samples were flipped for each melting cycle in order to improve chemical homogeneity. The arc current was kept constant at 120 A in all melting and remelting

Table 1 The different alloy systems produced in the present effort along with their nominal, actual overall (EDS mapping) and phase (EDS point identification) compositions

		Atomic percentage at.%		
		Al	Ni	Cr
Alloy A	NOMINAL	37.5	37.5	25
AlNi–25Cr	ACTUAL	32.53	41.54	25.93
(Hypo-eutectic)	LIGHT (PRIMARY)	41.74	49.52	8.73
	DARK	11.13	62.94	25.92
		Al	Ni	Cr
Alloy B	NOMINAL	33.5	33.5	33
AlNi–33Cr	ACTUAL	28.56	37.82	33.62
(Eutectic)	LIGHT (PRIMARY)	37.9	50.51	11.58
	DARK	9.68	28.92	61.40
		Al	Ni	Cr
Alloy C	NOMINAL	27.5	27.5	45
AlNi–45Cr	ACTUAL	22.55	31.37	46.09
(Hyper-eutectic)	DARK	8.8	9.7	81.5
	LIGHT	33.41	47.99	18.6
		Al	Ni	Cr
Alloy D	NOMINAL	20	20	60
AlNi–60Cr	ACTUAL	16.72	23.07	60.21
(Hyper-eutectic)	LIGHT	30.5	48.95	20.55
	DARK	8.81	9.22	81.97
		Al	Ni	Cr
Alloy E	NOMINAL	10	10	80
AlNi–80Cr	ACTUAL	6.87	10.58	82.54
(Hyper-eutectic)	DARK	30.7	55.87	13.43
	LIGHT	4.08	4.27	91.65

Table 2 The different alloy systems with Mo added produced in the present effort along with their nominal, actual overall (EDS mapping) and phase (EDS point identification) compositions

		Atomic percentage at.%			
		Al	Ni	Cr	Mo
Alloy F	NOMINAL	37	37	20	6
AlNi–20Cr–6Mo	ACTUAL	32.86	40.59	19.98	6.57
(Hypo-eutectic)	DARK (PRIMARY)	41.7	50.95	6.77	0.58
	LIGHT	11.86	9.19	56.29	22.64
		Al	Ni	Cr	Mo
Alloy G	NOMINAL	33.5	33.5	28.75	5
AlNi–28.75Cr–5Mo	ACTUAL	29.1	35.89	29.57	5.44
(Near eutectic)	DARK	38.14	48.25	12.38	1.22
	LIGHT	11.07	11.8	67.07	10.05
		Al	Ni	Cr	Mo
Alloy H	NOMINAL	33	33	28	6
AlNi–28Cr–6Mo	ACTUAL	28.41	35.8	29.35	6.44
(Near eutectic)	DARK	39.7	49.8	9.9	0.55
	LIGHT	8.43	10.48	68.33	13.05

steps. Argon (industrial purity) was used as protective atmosphere and a Ti gutter was in all cases melted first in order to further reduce oxygen contamination phenomena. This manufacturing process is considered to be a standard practice for production HEAs and has been widely used in other research efforts as for example in [20]. The actual composition was checked using EDS mapping in the SEM in at least 3 different locations of lower magnification and all fell within the measured compositions presented in Tables 1 and 2.

The relative ratio of Ni and Al, in alloy systems, was kept constant and atomically equal. All alloy compositions are in at.%. The presentation of both nominal and actual compositions is a common practice as in many cases a divergence between them is met, as in the case of the work of Sheng et al. [21].

The microstructure of the alloys were studied in their as cast condition. Crystal structure of the HEA was examined with an X-ray diffractometer (Bruker, D8 Advance) using a scanning rate of 0.01°/s. The metallographic specimens were mounted in bakelite, abraded on SiC papers up to 2400 grit and then polished with a 3 μm diamond suspension. The polished specimens were etched using aqua regia. Alloy's microstructure was analyzed with the use of a Scanning Electron Microscope (JEOL 6510 LV) equipped with both backscatter electron (BSE) and energy dispersive spectroscopy (EDS) detector of X-Act type by Oxford Instruments.

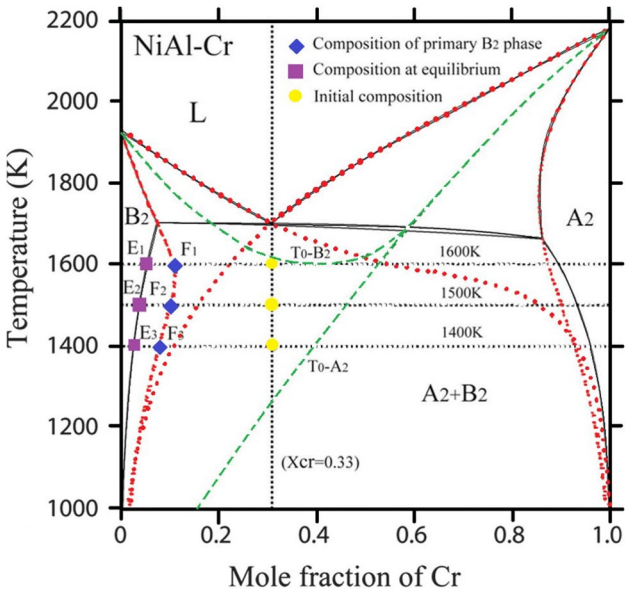

Fig. 1 Graphical representation of Tang's et al. [1] pseudo-binary phase diagram

3 Results and discussion

3.1 Microstructure

Prior to any attempt for the explanation of the received microstructures and since the work is based on the work of Tang et al. [1], a graphical representation of their NiAl–Cr pseudo-binary phase diagram is graphically presented in Fig. 1.

Figure 2a–e shows the panoramic view of the microstructure of the different Ni–Al–Cr alloys produced in the present effort and Table 1 presents the results of the EDS point analysis on the various phases formed for each individual alloy system. Figure 2a–e and Table 2 present the microstructure and EDS point analysis of the Ni–Al–Cr–Mo alloys, respectively. Figures 3 and 4 present the XRD patterns of the alloys A (NiAl–25Cr), B (NiAl–33Cr) D (NiAl–60Cr) and F (AlNi–20Cr–6Mo), G (NiAl–28.75–5Mo), H (NiAl–28Cr–6Mo) respectively. Clearly, a variety of phases and morphological features can be distinguished for each case.

3.1.1 Alloy A

According to the equilibrium NiAl–Cr pseudo-binary phase diagram [1], alloy A is of hypo-eutectic composition and as such, primary NiAl phase followed by the formation of eutectic micro-constituent should be observed. Indeed, as shown in Fig. 2a, the microstructure consists of primary dendrites with dark spots dispersed and fine fibrous eutectic phase. Between the light primary and the

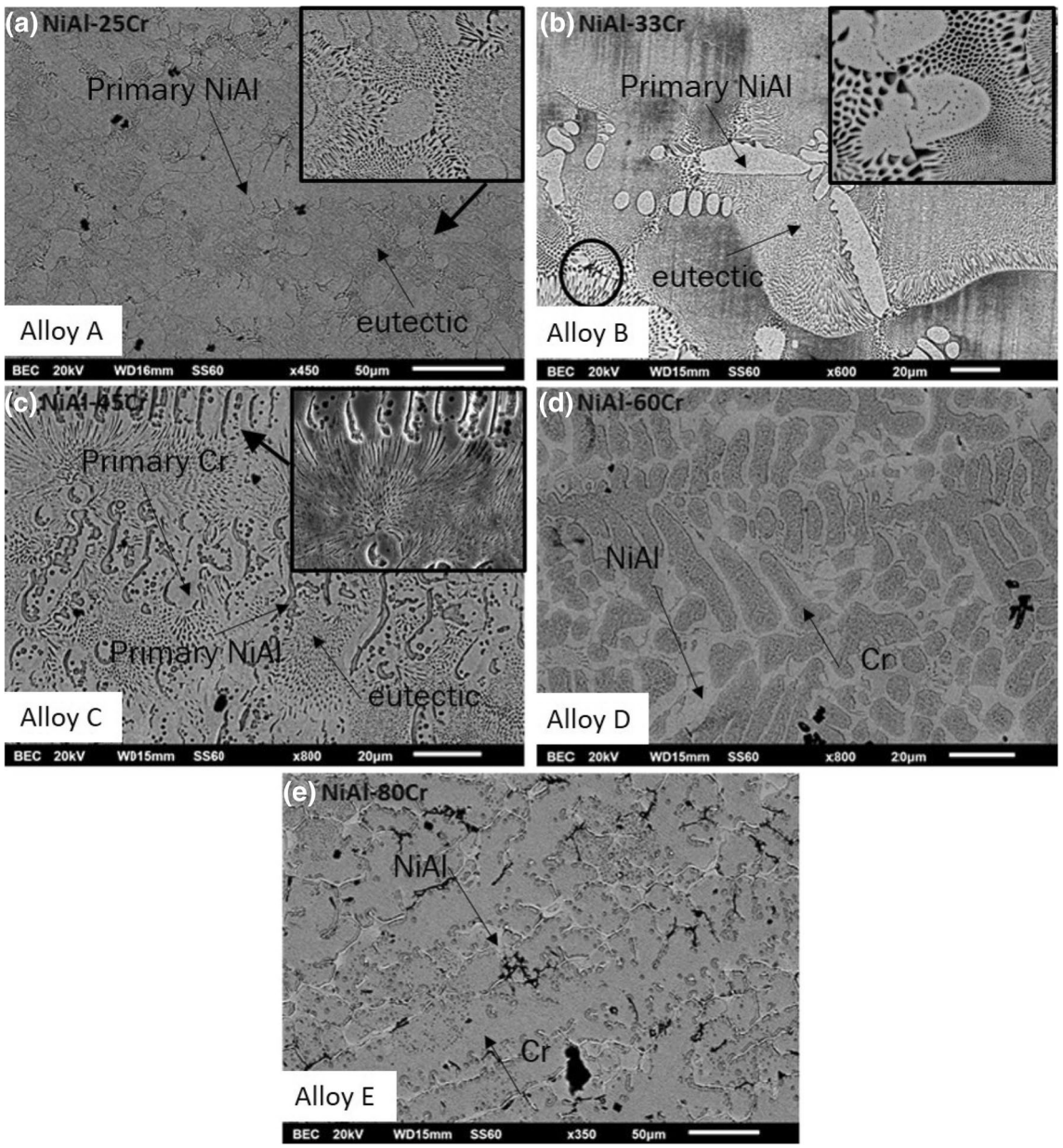

Fig. 2 The microstructures of the different systems produced in the present effort under SEM–EDS examination: **a** Alloy A (NiAl–25Cr hypo-eutectic alloy), **b** Alloy B (NiAl–33Cr eutectic alloy), **c** Alloy C (NiAl–45Cr hyper-eutectic alloy), **d** Alloy D (NiAl–60Cr hyper-eutectic alloy) and **e** Alloy E (NiAl–80Cr hyper-eutectic alloy)

eutectic phases a thin dark phase is present and it seems that the eutectic constituent nucleates on this. EDS analysis of the primary phase (Table 1) revealed that this phase is enriched in Ni and Al, with a great amount of Cr being dissolved within. On the contrary, the dark spots into the primary dendrites are rich in Cr. The dark fibrous phase of the eutectic micro-constituent as well as the halo like dark phase around the primary, is Cr rich with a significant quantity of Ni (mostly) and Al (less) dissolved. The presence of two phases, one BCC with lattice parameter a = 2.8832 Å that corresponds to Cr and a second BCC(B2) with lattice parameter a = 2.8888 Å that corresponds to NiAl, is confirmed by the XRD patterns presented on Fig. 4.

3.1.2 Alloy B

Alloy B is of slightly hypo-eutectic composition according to Peng et al. [22] calculated liquidus surface projection of the Al–Cr–Ni system and, as shown in Fig. 2b, consists of light primary dendrites and fine fibrous eutectic structure. EDS analysis showed that the primary phase is rich in Ni, Al with greater amounts (than the

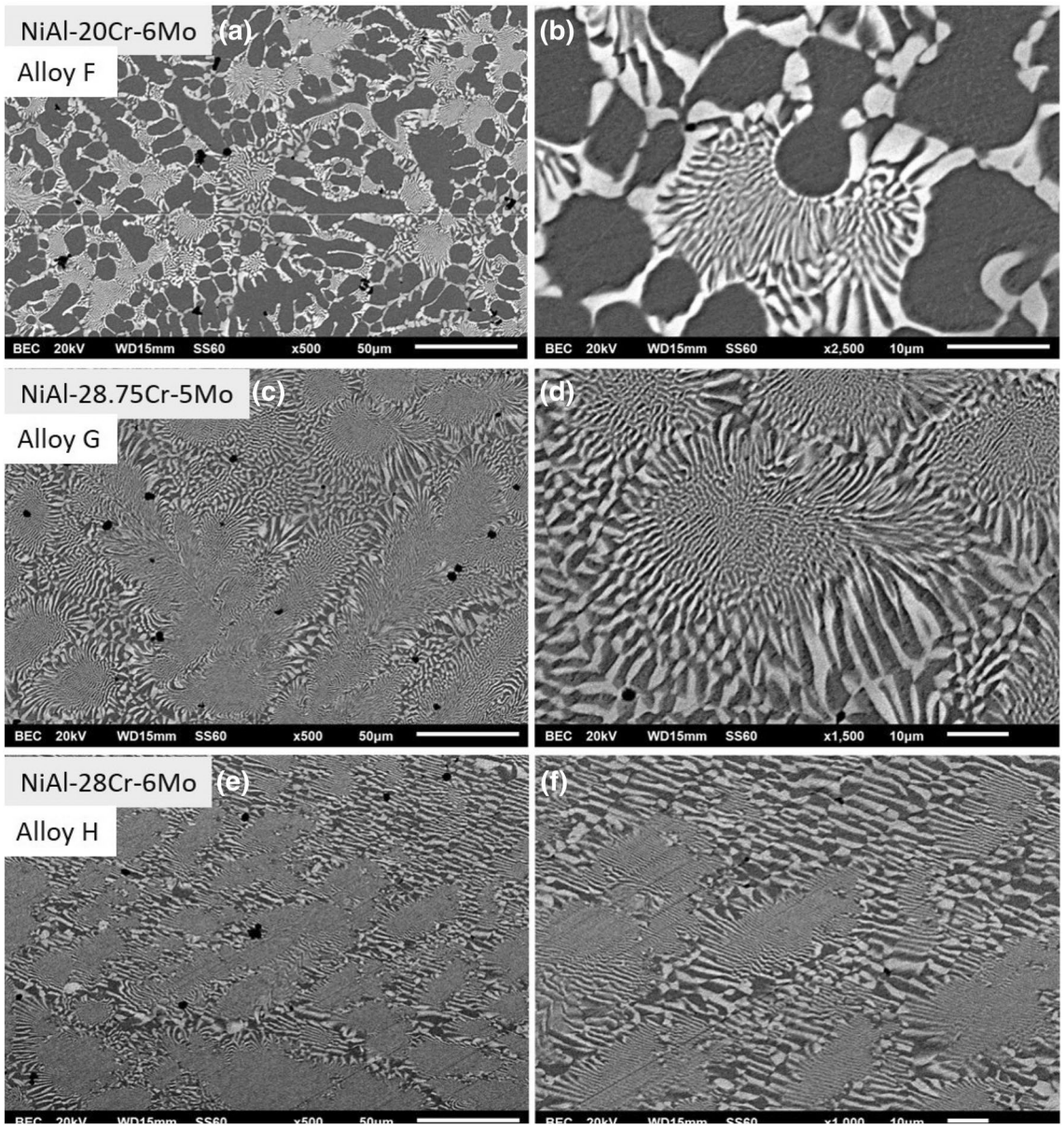

Fig. 3 The microstructures of the different Ni–Al–Cr–Mo systems produced in the present effort under SEM–EDS examination: **a**, **b** Alloy F (AlNi–20Cr–6Mo), **c**, **d** Alloy G (NiAl–28.75–5Mo), **e**, **f** Alloy H (NiAl–28Cr–6Mo alloy)

alloy A) of dissolved Cr. The eutectic structure is also fine with fibrous Cr rich phase and becomes a little coarser at the end of the solidification (at grain boundaries). It is obvious in Fig. 1b that the thin dark phase (also rich in Cr) exists also in this alloy around the primary NiAl dendrites. As in the case of alloy A the dark Cr rich spot like phase is present into the primary dendrites. The XRD pattern, as in the previous case, confirms the Cr and NiAl phases (Fig. 4).

3.1.3 Alloy C

Alloy C (Fig. 1c) is of composition that corresponds to the hyper-eutectic side of the pseudo-binary NiAl–Cr equilibrium phase diagram. It consists of altering light and dark phases in the primary dendrites and of eutectic structure where the Cr rich phase is solidified in a rod like mode at the center of the eutectic grain, becoming coarser and lamellar at the grain boundaries. The dark primary phase

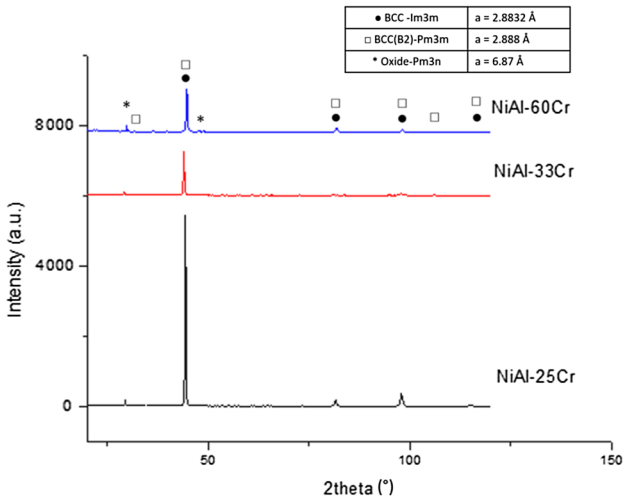

Fig. 4 The XRD patterns of the alloys A (NiAl–25Cr), B (NiAl–33Cr) and D (NiAl–60Cr)

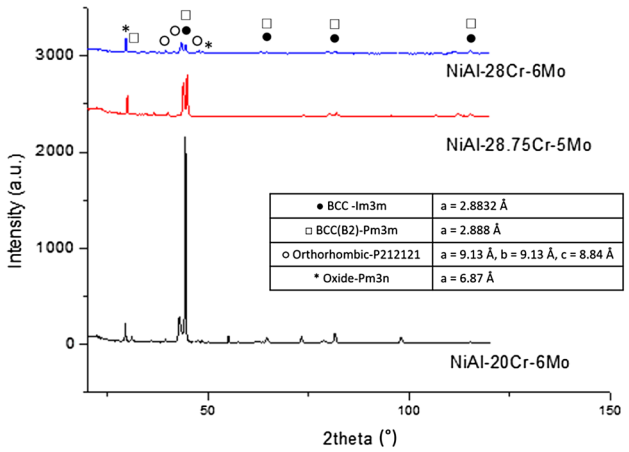

Fig. 5 The XRD patterns of the alloys F (AlNi–20Cr–6Mo), G (NiAl–28.75–5Mo), H (NiAl–28Cr–6Mo)

consists also of secondary light and dark altering phases. The EDS analysis revealed that the primary altering light and dark phases as well as the secondary ones into the primary dendrites are rich in Ni, Al (light) and Cr (dark) (Table 1).

3.1.4 Alloy D

Dark primary dendrites is the main microstructural feature of this hyper-eutectic alloy shown in Fig. 2d with light inter-dendritic areas. The primary dendrites are rich in Cr and the light are rich in Ni, Al. Between these primary phases, small eutectic grains exist. As in the case of alloy C, altering light and dark phases into the primary dark phase are also observed. The XRD pattern confirms also in this case the Cr and NiAl phases (Fig. 4).

3.1.5 Alloy E

The last NiAl–Cr alloy is also a hyper-eutectic one, with Cr content up to 80%. This alloy (Fig. 2e) shows a microstructure where the light primary dendrites are rich in Cr, and the inter-dendritic small areas are rich in NiAl. The Cr content into the NiAl constituent is as high as 9%. Dark spots are dispersed into the primary dendrites and EDS analysis showed that these dark spots are NiAl (Fig. 3).

3.1.6 Alloy F

The alloy F is of hypo-eutectic composition according to Peng et al. [22]. The microstructure is shown in Fig. 3a and b, and consists of primary dark dendrites. A light halo-like phase around the primary dendrites and finally a lamellar eutectic microstructure are identified. EDS analysis depicted that the dark phase is rich in NiAl and the light rich in Cr, Mo. Cr and Mo are dissolved in contents of 6.77% and 0.58%, respectively, into the NiAl phase and NiAl in content of about 10% into the Cr–Mo rich phase. The XRD patterns (Fig. 5) revealed the presence of another phase of orthorhombic structure corresponding to MoNi intermetallic.

3.1.7 Alloys G, H

For G and H alloys, it is obvious in Fig. 3c, d and in Fig. 3e, f respectively, that the microstructure is identified as eutectic with very fine lamellas at the center of the grains that become coarser at the grain boundaries. EDS analysis of the light and dark phases are shown in Table 2. The presence of the MoNi intermetallic is also evident in both G and H alloys.

4 Solidification sequence and remarks

4.1 Ni–Al–Cr alloys

4.1.1 Alloy A

As mentioned previously, Alloy A is of hypo-eutectic composition and as such, primary NiAl phase followed by the formation of eutectic micro-constituent is observed. The evolution of this microstructure, nevertheless, should also be approached in terms of important factors such as undercooling and recalescence and not only on equilibrium condition considerations. In this effort, the authors used a fast solidification technique to investigate how undercooling and recalescence affect the final

microstructure. The big amounts of Cr into B2 (NiAl) phase (approximately 9%) and respectively of Ni and Al into Cr rich phase are remarkable. According to Tang et al. [1], for the composition of Alloy A, the T0-B2 (practically the maximum temperature necessary for the onset of the B2 (NiAl) phase nucleation in a partitionless way) is much higher than that of the T0-A2 (Cr phase) corresponding one. As the primary dendrites grow, heat is released, due to recalescence, ahead of their front, which alters the solidification kinetics. The temperature gradient is altered and conditions where partitionless growth becomes partitioning are established. This slower growth mode leads to the rejection of Cr around the dendrite core forming a Cr rich layer (dark phase) outside the dendrite boundaries. This Cr rich phase in turns, rejects the NiAl phase and eutectic solidification conditions are established for the rest of the liquid phase. High undercooling conditions at the areas where the formation of the eutectic structure begins, in conjunction with the cooling rates experienced upon manufacturing, lead to the formation of fibrous like eutectic morphologies. As the solidification comes to the end, recalescence and heat release, in a second instance, raise the remaining liquid temperature, the solidification velocity slows down and conditions of more effective diffusion are established, leading to coarser structures.

The Cr content into the primary NiAl dendrites is as high as roughly 9–10%, which is much higher than the equilibrium one. These supersaturated (in Cr) NiAl dendrites, as the alloy is cooled, undergo a spinodal decomposition, transforming into a more stable condition where fine (with a size of 1 μm or less) Cr rich spot like phases are created. Tang et al. [1] have predicted and Guo et al. [23] and Ananiades et al. [24] have reported similar decomposition sequences.

4.1.2 Alloy B

The case of alloy B is similar to that of the alloy A. According to the equilibrium diagram, as shown by Tang et al. [1], Alloy B is of hypo-eutectic composition and as such a NiAl primary phase takes place. EDS analysis of these primary dendrites showed enrichment in Ni and Al with Cr being present in a reasonable amount. The obtained microstructure shows that the expressed undercooling is lower than T0-B2 which implies that B2 with an amount of dissolved Cr is primarily formed. It is worth noticing that, as Table 1 additionally shows, the primary B2 phase contains higher amounts of dissolved Cr which is a result of more intensive solute trapping effect. As in the case of alloy A, at the end of the dendrite solidification, due to the partitioning mode, a thin Cr rich phase appears around the primary dendrites. Upon the formation of the primary B2 phase, heat is released due to recalescence in the remaining liquid, temperature is raised upon the T0-B2 value and conditions for eutectic undercooling are established leading to the formation and growth of eutectic constituent. Alterations of the eutectic morphology from fibrous to coarser configurations, are also evident with the mechanism of such modification being similar to that presented in the previous paragraph. As in the Alloy A case, at low temperatures the supersaturated primary dendrites decompose and create the dark rich in Cr spots.

4.1.3 Alloy C

Alloy C has a composition that corresponds to the hyper-eutectic side of the pseudo-binary NiAl–Cr equilibrium phase diagram [1]. In this case, primary Cr dendrites should be expected to form. The microstructure, nevertheless (Fig. 2c), is by far more complicated. As Fig. 2c depicts, large dendritic like morphologies can be observed consisting of alternating B2 and A2 phases and being developed almost perpendicular to the dendritic primary axis. A eutectic structure is also evident. Despite the obscurity of the microstructure, Tang et al. [1] predictions can provide a vital information on this characteristic feature. According to their work, for this composition, the T0-B2 is still higher than that of T0-A2 but their difference is significantly reduced. Both T0-B2 and T0-A2 persist to be lower than the Te temperature. Based on this observation the most credible solidification scenario could be as follows: The undercooling upon the onset of solidification falls below the T0-A2 point and as such primary A2 phase starts to form trapping Ni and Al. However, since the T0-B2 and T0-A2 gap is considerably narrow, local release of heat of recalescence ahead of the growing A2 phase, establishes undercooling conditions for the development of B2 phase that also traps Cr. In such manner, alternating A2-B2 phase configurations are formed. Similar phenomena have been observed in various research efforts dealing with regular and anomalous eutectic solidification [25–31]. Further recalescence causes temperature increase in the remaining liquid phase and eutectic growth commences. The eutectic structure follows similar patterns as described in the previous cases. As Table 1 shows, both the dark and the light phases are supersaturated. As the temperature falls they undergo a spinodal decomposition. In the light phase it appears like spots (as in the A and B alloys) but in the case of the dark phase it is more intense, the altering light and dark phases being greater (a size of about 2 μm).

4.1.4 Alloy D

The vital importance of the T0-B2 and T0-A2 relation with the eutectic temperature Te, is depicted in the case of Alloy D. This system is a hyper-eutectic alloy and

as such a primary A2 phase and a eutectic constituent should be expected. However, as Fig. 2d shows, this is not the case. The microstructure consists of A2 and B2 phases with the eutectic phase being practically vanished. The predictions of Tang et al. [1] are also applicable in this case. According to them, T0-B2, T0-A2 and Te almost coincide. This coincidence brings the system at maximum confusion upon the onset of solidification. Undercooling causes a parallel de-coupled growth of the A2 and B2 phases allowing no time and space for the development of a eutectic constituent. In the case of this alloy, the spinodal decomposition can also be observed. The altering light and dark phases into the primary dark dendrites, as well as the dark spots into the light primary phase, are more intensively present.

4.1.5 Alloy E

Similar, as in the previous cases, trends seem to have been followed for Alloy E, which is also a hyper-eutectic alloy. T0-A2 and T0-B2, according to Tang et al. [1] coincide and are far above the Te. As such, during solidification and up to its completion, even in small undercooling, a parallel growth of both B2 and A2 phase takes place leading to the microstructural configuration observed in Fig. 2e with no trace of eutectic constituent. EDS analysis showed that the dendrites are rich in Cr and the inter-dendritic area rich in NiAl. The dark spots observed in the primary dendritic areas are NiAl spinodaly decomposed of the Cr rich matrix at lower temperatures.

Prior to the presentation of the Mo containing alloys, a general remark should be addressed concerning the microstructures of alloys A-to-G. A closer examination of the XRD diagrams shows the existence of lower intensity peaks the nature of which is difficult to be ascertained. Similar peaks have also been reported in the works of Sheng et al. [32, 33] where have been identified as σ, μ or even Ni_3Al phases. In the present effort local segregation of Cr, as proposed by Sheng et al. [32, 33], may indeed cause the formation of σ and μ phases which however cannot be clearly identified due to the lack of TEM examination. According to Sheng et al. [32, 33], another potential source of these lower intensity peaks could be the formation of Ni_3Al lathes when the Ni–Al ratio diverges form the equiatomic proportion and in favor of the Ni content. Indeed the actual alloy compositions (Table 1) do reveal this type of divergence, however the characteristic morphology of Ni_3Al lathes as clearly presented in the Sheng et al. [32] cannot be spotted in the present microstructures. It is thus logical to assume that if Ni_3Al is formed it must be at such restricted amounts that, at least microstructurally, cannot be distinguished.

4.2 Ni–Al–Cr–Mo alloys

4.2.1 Alloy F

The microstructure of alloy F as shown in Fig. 3a and b, consists of primary B2 dendrites as it is depicted by the EDS analysis shown in Table 2, Cr is dissolved in about 6.7 at.% into the primary B2 phase. A white Cr, Mo rich phase around the primary NiAl phase and finally a eutectic microstructure are identified. Obviously, NiAl has the first role in the solidification that takes place at an undercooling temperature a little lower than that of T0-B2. The small quantities of the trapped Cr verify this assumption. Even though Mo is the element with the higher melting temperature, it is present in a very small quantity. As the primary dendrites have been solidified, the liquid gets to a hyper-eutectic composition and a Cr, Mo rich primary phase is solidified either around the primary NiAl or inter-dendritically. This CrMo rich phase is located there where the eutectic structure nucleates. The recalescence on the front is high (Mo has a great value of latent heat of fusion) and creates conditions for eutectic solidification in the rest of the liquid phase. The eutectic microstructure appears with fine lamellas. The microstructure is in complete agreement with the calculated liquidus surface projection of the NiAl–Cr–Mo system proposed by Peng et al. [22] that gives primary NiAl phase for the given composition. Regarding the MoNi intermetallic existence, the authors believe that there are two different paths for its formation. On the first case as the primary NiAl dendrites solidification is about to be completed, the excessive Ni (see Table 2) concentration reacts with Mo in a peritectic way and the MoNi intermetallic is the reaction's product, as the binary Mo–Ni phase diagram also depicts [34]. It should be noticed that the peritectic reaction between Mo and Ni can happen in Mo–Ni proportions from Mo 97 at.%–Ni 3 at.% up to about Mo 50 at.%–Ni 50 at.%. The second path for MoNi formation is during the eutectic solidification: The eutectic phases are supersaturated (CrMo in NiAl and NiAl in CrMo) as it has been mentioned before, due to fast solidification conditions. Ni is also in excessive proportion than the required for NiAl intermetallic formation. Ni and Mo exist in both phases and react directly to give MoNi intermetallic phase.

4.2.2 Alloys G and H

For G and H alloys, as it can be seen in Fig. 3c, d and Fig. 3e, f, the microstructure is identified as eutectic with very fine lamellas at the center of the grain. The solidification takes place at small undercooling at temperature over the T0 B2, T0 A2 in eutectic conditions. As the growth velocity slows, due to recalescence released heat in front of the

solid–liquid interface, the lamellar spacing increases and the fine lamellas become coarser at the end of solidification. Similar coarsening has been reported by other works as well [28, 35, 36]. For the alloys F, G and H, no rod or fibrous like Cr solidification has been observed. The Mo addition in the G and H alloys caused a liquidus temperature raise as it is obvious by the Cr–Mo binary phase diagram [37]. The melting conditions were the same for all the alloys and the temperature over the melting temperature that was achieved was the same. As the melting temperature is raised, the overheating temperature is smaller and the respective undercooling lower. Similar conditions of overheating and corresponding undercooling have been reported by Mei et al. [38] and Yang et al. [39].

As a consequence of the previous observations, the T0-B2 and T0-A2 temperatures also raise. This temperature increase in conjunction with the lower achieved undercooling, leads to the establishment of a nucleation temperature over T0-B2 and T0-A2 and eutectic solidification is evident. For both the G and H alloys the MoNi intermetallic is formed in a manner similar to the second path of the previous case.

As in the previous systems (no Mo additions), potential formation of σ, μ and Ni_3Al lathes at small extent can also be formed, as described in previous paragraphs.

A general comment on the solidification behavior of the produced alloys in the present effort, is associated with the influence of the cooling rate experienced upon solidification. As Sheng et al. [40–43] correctively mention in their efforts, rapid cooling can cause to a significant degree of microstructural alterations when compared to conventional casting conditions. Despite the fact that such type of comparison did not conducted in the present work, it is quite reasonable to assume that some of the structural refinement and primary phase formation and preservation observed in the microstructures of the produced alloys, are exactly due to the fast solidification conditions as Sheng et al. [40–43] also reported.

5 Concluding remarks

- The predictions of Tang et al. [1] concerning the NiAl–Cr system, seem to be micro-structurally verified, for all the different alloy compositions, varying from hypo- to hyper-eutectic elemental ratios.
- T0 temperatures, undercooling and recalescence phenomena are responsible for the primary NiAl phase establishment, observed in alloys A and B (hypo-eutectic alloys)
- The significance of the T0 temperatures is especially noticed in the case of alloy C which as an hyper-eutectic alloy, does not reveal a sole Cr based primary phase, but an alteration of A2 and B2 primary phases along with eutectic micro-constituent
- The role T0 temperature in restricting the formation of eutectic morphologies, is revealed in the case of alloys D and E.
- The Cr substitution by Mo at the F, G and H alloys causes T0-B2 and T0-A2 temperatures to increase. The lower undercooling conditions as well as the recalescence and the heat release during the CrMo rich phase solidification, establish conditions of temperature higher than T0-A2 and T0-B2 and normal eutectic solidification takes place. This heat release is also responsible for the lamellar solidification of Cr in the eutectic microstructure.

Acknowledgements This research is co-financed by Greece and the European Union (European Social Fund-ESF) through the Operational Programme «Human Resources Development, Education and Lifelong Learning» in the context of the project "Strengthening Human Resources Research Potential via Doctorate Research" (MIS-5000432), implemented by the State Scholarships Foundation (IKY).

Compliance with ethical standards

Conflict of interest The authors would like to confirm that there is no conflict of interest.

References

1. Tang B, Cogswell DA, Xu G, Milenkovic S, Cui Y (2016) Formation mechanism of eutectic microstructure in NiAl–Cr composites. Phys Chem Chem Phys 18(29):19773–19786
2. Laughlin DE, Hono K (2014) Physical metallurgy, vol 1, 668. Elsevier, Amsterdam. ISBN: 978-0-444-59598-0
3. Noebe RD, Bowman RR, Nathal MV (1994) Physical and mechanical metallurgy of NiAl, NASA technical paper 3398
4. Takeuchi A, Inoue A (2005) Classification of bulk metallic glasses by atomic size difference, heat of mixing and period of constituent elements and its application to characterization of the main alloying element. Mater Trans 46(12):2817–2829
5. Locci IE, Dickerson RM, Grag A, Noebe RD, Whittenberger JD, Nathal MV, Darolia R (1996) Microstructure and phase stability of single crystal NiAl alloyed with Hf and Zr. J Mater Res 11:3024
6. Miracle DB (1993) The physical and mechanical properties of NiAl. Acta Mater 41:649
7. Barabash RI, Liu W, Tischler JZ, Bei H, Budai JD (2012) Phase-specific elastic/plastic interface interactions in layered NiAl–Cr(Mo) structures. Acta Mater 60:3279
8. Chen ST, Tang WY, Kuo YF, Chen SY, Tsau CH, Shun TT, Yeh JW (2010) Microstructure and properties of age-hardenable AlxCrFe1.5MnNi0.5 alloys. Mater Sci Eng A 527(21–22):5818–5825
9. Hsu CY, Juan CC, Sheu TS, Chen SK, Yeh JW (2013) Effect of aluminum content on microstructure and mechanical properties of AlxCoCrFeMo0.5Ni high-entropy alloys. J Met 65:1840–1847
10. Hsu CY, Sheu TS, Yeh JW, Chen SK (2010) Effect of iron content on wear behavior of AlCoCrFexMo0.5Ni high-entropy alloys. Wear 268:653–659

11. Wu JM, Lin SJ, Yeh JW, Chen SK, Huang YS, Chen HC (2006) Adhesive wear behavior of AlxCoCrCuFeNi high-entropy alloys as a function of aluminum content. Wear 261(5–6):513–519
12. Chuang MH, Tsai MH, Wang WR, Lin SJ, Yeh JW (2011) Microstructure and wear behavior of AlxCo1.5CrFeNi1.5Tiy high-entropy alloys. Acta Mater 59:6308–6317
13. Munitz A, Meshi L, Kaufman MJ (2017) Heat treatments' effects on the microstructure and mechanical properties of an equiatomic Al–Cr–Fe–Mn–Ni high entropy alloy. Mater Sci Eng A 689:384–394
14. Cline HE, Walter JL (1970) The effect of alloy additions on the rodplate transition in the eutectic NiAl–Cr. Metall Trans 1(10):2907–2917
15. Demirtas H, Gungor A (2015) Effect of alloying elements on the microstructure and mechanical properties of NiAl–Cr(Mo) eutectic alloy. Int Sci J Mater Sci Non-Equilib Phase Transform 1(2):25–29
16. Shang Z, Shen J, Zhang J, Wang L, Wang L, Fu H (2014) Effect of microstructures on the room temperature fracture toughness of NiAl–32Cr–6Mo hypereutectic alloy directionally solidified at different withdrawal rates. Mater Sci Eng A 6(11):306–312
17. Yang J-M, Jeng SM, Bain K, Amato RA (1997) Microstructure and mechanical behavior of in situ directional solidified NiAl/Cr(Mo) eutectic composite. Acta Mater 45(1):295–305
18. Tang L-Z, Zhang Z-G, Li S-S, Gong S-K (2010) Mechanical behaviors of NiAl–Cr(Mo)-based near eutectic alloy with Ti, Hf, Nb and W additions. Trans Nonferr Met Soc China 20:212–216
19. Wang L, Shen J, Zhang Y, Xu H, Fu H (2016) Microstructure and mechanical properties of NiAl-based hypereutectic alloy obtained by liquid metal cooling and zone melted liquid metal cooling directional solidification techniques. J Mater Res 31(5):646–654. https://doi.org/10.1557/jmr.2016.61
20. Zheng L, Sheng LY, Qiao YX, Yang Y, Lai C (2019) Influence of Ho and Hf on the microstructure and mechanical properties of NiAl and NiAl–Cr(Mo) eutectic alloy. Mater Res Express 6(4):046502
21. Sheng LY, Yang F, Xi TF, Zheng YF, Guo JT (2013) Microstructure and room temperature mechanical properties of NiAl–Cr(Mo)–(Hf, Dy) hypoeutectic alloy prepared by injection casting. Trans Nonferr Met Soc China 23(4):983–990
22. Sheng LY, Du BN, Zan SP, Lai C, Jiao JK, Gao YB, Xi TF (2018) Optimization of the microstructure and mechanical properties of a Laves phase-strengthened hypoeutectic NiAl/Cr(Mo, W) alloy by suction casting. Strength Mater 5(3):504–514
23. Peng J, Franke P, Seifert HJ (2016) Experimental investigation and CALPHAD assessment of the eutectic trough in the system NiAl–Cr–Mo. J Phase Equilib Diffus 37(5):592–600
24. Guo S, Ngand C, Liu CT (2013) Sunflower-like solidification microstructure in a near-eutectic high-entropy alloy. Mater Res Lett 1(4):228–232
25. Ananiadis E, Lentzaris K, Georgatis E, Mathiou C, Poulia A, Karantzalis AE (2019) AlNiCrFeMn equiatomic high entropy alloy: a further insight in its microstructural evolution, mechanical and surface degradation response. Met Mater Int 8:8–9. https://doi.org/10.1007/s12540-019-00401-4
26. Kattamis TZ, Flemings MC (1970) Structure of undercooled Ni–Sn eutectic. Metall Trans 1:1449
27. Wei B, Herlach DM, Feuerbacher B, Sommer F (1993) Dendritic and eutectic solidification of undercooled Co–Sb alloys. Acta Mater 41(6):1801–1809
28. Li M, Kuribayashi K (2016) Free solidification of undercooled eutectics. Mater Trans 47(12):2889–2897
29. Yang C, Gao J, Zhang YK, Kolbe M, Herlach DM (2011) New evidence for the dual origin of anomalous eutectic structures in undercooled Ni–Sn alloys: in situ observations and EBSD characterization. Acta Mater 59:3915–3926
30. Liu L, Wei XX, Huang QS, Li JF, Cheng XH, Zhou YH (2012) Anomalous eutectic formation in the solidification of undercooled Co–Sn alloys. J Cryst Growth 358:20–28
31. Goetzinger R, Barth M, Herlach DM (1998) Mechanism of formation of the anomalous eutectic structure in rapidly solidified Ni–Si, Co–Sb and Ni–Al–Ti alloys. Acta Mater 46(5):1647–1655
32. Karma A (1998) Model of grain refinement in solidification of undercooled melts. Int J Non-Equiulib Process 1(2):201–233
33. Sheng LY, Xie Y, Xi TF, Guo JT, Zheng YF, Ye HQ (2011) Microstructure characteristics and compressive properties of NiAl-based multiphase alloy during heat treatments. Mater Sci Eng A 528(29-30):8324–8331
34. Sheng L, Wang L, Xi TF, Zheng Y, Ye H (2011) Microstructure, precipitates and compressive properties of various holmium doped NiAl/Cr(Mo, Hf) eutectic alloys. Mater Des 32(10):4810–4817
35. http://resource.npl.co.uk/mtdata/phdiagrams/moni.htm
36. Tan Y, Li J, Wang J, Kou H (2017) Seaweed eutectic-dendritic solidification pattern in a CoCrFeNiMnPd eutectic high-entropy alloy. Intermetallics 85:74–79
37. Clopet CR, Cochrane RF, Mullis AM (2013) The origin of anomalous eutectic structures in undercooled Ag–Cu alloy. Acta Mater 61:6894–6902
38. http://resource.npl.co.uk/mtdata/phdiagrams/crmo.htm
39. Mei Q, Li J (2015) Dependence of liquid supercooling on liquid overheating levels of Al small particles. Materials 9(1):1–8. https://doi.org/10.3390/ma9010007
40. Yang B, Perepezko Jürn JH, Schmelzer WP, Gao YL (2014) Dependence of crystal nucleation on prior liquid overheating by differential fast scanning calorimeter. J Chem Phys 140:104513. https://doi.org/10.1063/1.4868002
41. Sheng LY, Yang F, Xi TF, Zheng YF, Guo JT (2012) Improvement of compressive strength and ductility in NiAl–Cr(Nb)/Dy alloy by rapid solidification and HIP treatment. Intermetallics 27:14–20
42. Guo JT, Xie Y, Sheng LY, Zhou LZ, Liang YC (2011) Effect of withdrawal rate on microstructure and mechanical properties of a directionally solidified NiAl-based hypoeutectic alloy doped with trace Hf and Ho. Intermetallics 19(2):206–211
43. Sheng LY, Guo JT, Ye HQ (2009) Microstructure and mechanical properties of NiAl–Cr(Mo)/Nb eutectic alloy prepared by injection-casting. Mater Des 30(4):964–969